

UC Santa Cruz

UC Santa Cruz Previously Published Works

Title

Seismological implications of a lithospheric low seismic velocity zone in Mars

Permalink

<https://escholarship.org/uc/item/1100n3f7>

Journal

Physics of the Earth and Planetary Interiors, 240

ISSN

00319201

Authors

Zheng, Yingcai
Nimmo, Francis
Lay, Thorne

Publication Date

2015-03-01

DOI

10.1016/j.pepi.2014.10.004

Peer reviewed

1 Seismological implications of a lithospheric low 2 seismic velocity zone in Mars

3 Yingcai Zheng^{a•}, Francis Nimmo^b, Thorne Lay^b

4
5 ^a *Earth Resources Laboratory, Massachusetts Institute of Technology, Cambridge, MA 02139, USA*

6 ^b *Department of Earth and Planetary Sciences, University of California Santa Cruz, Santa Cruz, CA*
7 *95064, USA*

8

10 **Abstract**

11 Most seismological models for the interior of Mars lack an upper mantle low velocity zone.
12 However, there is expected to be a large thermal gradient across the stagnant conductive lid
13 (lithosphere) of Mars. This gradient should tend to decrease elastic wave velocities with increasing
14 depth, with this effect dominating the opposing tendency caused by increasing pressure with depth
15 because Mars has low gravity. An upper mantle lithosphere with a low velocity zone (LVZ) beneath a
16 thin high velocity “seismic lid” is thus predicted. The upcoming NASA InSight mission includes a
17 three-component seismometer, which should provide the first opportunity to directly detect any
18 lithospheric LVZ in Mars. Seismic wavefields expected for Mars mantle velocity structures with or
19 without a strong LVZ are very distinct. The LVZ models predict shadow zones for high-frequency
20 seismic body wave phases such as *P*, *S*, *PP* and *SS*, etc. The most diagnostic waves that can be used
21 to evaluate presence of a lithospheric LVZ given a single seismometer are intermediate-period global
22 surface waves, which travel along the great circle from a seismic source to the seismometer. An LVZ
23 produces distinctive dispersion, with a Rayleigh wave Airy phase around 100 s period and very
24 different surface wave seismograms compared to a model with no LVZ. Even a single observation of
25 long-period surface waves from a known range can be diagnostic of the lithospheric structure.

• Corresponding author. Tel.: +1 617324 0268; fax: +1 617xxx xxxx. E-mail Address:
yczheng@mit.edu (Y. Zheng).

26 Establishing the existence of an LVZ has major implications for thermal evolution, volatile content
27 and internal dynamics of the planet.

28
29

30 **1. Introduction**

31 The seismological low-velocity zone (LVZ) in Earth's upper mantle, first proposed by Gutenberg
32 (1948; 1959), is closely linked to plate tectonics because it is related to thermal, volatile and
33 compositional effects associated with the rheological transition from the lithosphere to the
34 asthenosphere (e.g., Anderson, 1989; Stixrude and Lithgow-Bertelloni, 2005). An LVZ is simply a
35 region from which the seismic velocity increases in both the upwards and downwards directions.
36 Thermal modeling suggests the possible existence of a similar seismic LVZ within the lithosphere of
37 Mars (Mocquet and Menvielle, 2000; Rivoldini *et al.*, 2011; Nimmo and Faul, 2013). This Martian
38 LVZ would be different than Earth's, being most pronounced within the thermal boundary layer
39 rather than near its deepest levels. Establishing whether Mars has such an LVZ has important
40 implications for our understanding of the internal dynamics, volatile content and thermal evolution of
41 the Martian mantle.

42 In 2016, NASA's InSight (Interior exploration using Seismic investigations, geodesy and heat
43 transport) Martian lander will deploy a single 3-component seismometer and a heat flow probe to
44 study the planet's deep interior (Banerdt *et al.*, 2013). Hopefully the seismic instrument will couple
45 well to the surface and record broadband signals from sufficiently energetic sources that excite
46 broadband seismic wavefields. In anticipation of this seismic data collection proving successful and
47 high quality broadband recordings being obtained, we consider whether the presence of a lithospheric
48 LVZ should have significant manifestations in the seismic wavefield that would allow its detection

49 from a single sensor and (likely) sparse sources at various ranges. Many seismic models have been
50 proposed for Mars (Figure 1a) and most do not include an upper mantle LVZ (e.g., Okal and
51 Anderson, 1978; Franck and Kowalle, 1994; Sohl and Spohn, 1997; Zharkov and Gudkova, 2005;
52 Khan and Connolly, 2008; Walzer *et al.*, 2010). Notable exceptions are those of Mocquet and
53 Menvielle (2000) and Nimmo and Faul (2013).

54 The case for the existence of an LVZ within Mars is straightforward. If a stagnant conductive
55 thermal boundary layer, or “thermal lid” overlies a convective mantle (Toksöz and Hsui, 1978;
56 Ogawa and Yanagisawa, 2011), a large temperature gradient will develop across the lithosphere (as is
57 true for Earth’s thermal boundary layer). Unlike for Earth, the thermal effect, which tends to reduce
58 seismic velocity with increasing depth in the lithosphere, can overcome the competing effect of
59 increasing pressure due to the low gravity of Mars (Nimmo and Faul, 2013). This results in a net
60 decrease in seismic velocity with increasing depth within the thermal boundary layer. The magnitude
61 of velocity reduction in the LVZ is a function of the temperature gradient in the stagnant lithosphere,
62 which depends on the mantle potential temperature and the thermal lid thickness. Seismic velocity
63 models based on the temperature profile adopted by Bertka and Fei (1997) do not result in an LVZ.
64 This is because the temperature drop across the top 250 km of the lithosphere in that profile is only
65 about 300 K, much less than expected for a stagnant lid (e.g., Ogawa and Yanagisawa, 2011).
66 Mocquet and Menvielle (2000) assumed the presence of a thick stagnant lid and predicted an LVZ at
67 a depth of 200-400 km; some of the models displayed in Rivoldini *et al.* (2011) also have an LVZ for
68 a hot mantle (potential temperature > 1800K). Nimmo and Faul (2013) also predicted the presence of
69 an LVZ, though their main intent was to match the bulk tidal and dissipative properties of Mars.
70 Although Verhoeven *et al.* (2005) considered a stagnant-lid convection scenario, their lid was too

Yingcai Zheng 9/30/14 3:40 PM
Formatted: Highlight

71 thick (it extends to 400-550km depth) to result in a large thermal gradient with a prominent LVZ.

72 None of these papers considered the detailed seismological implications of an LVZ.

73 The NASA InSight mission will provide an important opportunity to test the existence of a
74 Martian lithospheric LVZ, if suitable seismic signals from as yet unknown sources are recorded. It is
75 not our intent here to carry out a detailed investigation of whether such sources are likely to exist, nor
76 to evaluate all possible causes of wavefield complexity such as 3D structure and anisotropy. Rather,
77 in the rest of this paper we present seismic wavefields computed for end-member global velocity
78 models for Mars with and without a lithospheric LVZ, guided by the model of Nimmo and Faul
79 (2013). Consideration of the computed seismic wavefields identifies diagnostic attributes that can be
80 sought for different epicentral ranges when long-period ground motion recordings for Martian
81 sources are obtained.

82 2. Seismological models for Mars

83 Planetary seismological models prescribe the compressional (P-wave) velocity, V_p , shear (*S*-
84 wave) velocity, V_s , density, and anelastic absorption factors, Q_p and Q_s for *P*- and *S*-waves,
85 respectively, as functions of depth. At present, there are no constraints on seismic anisotropy for
86 Mars, so usually isotropic models are considered.

87 The model we adopt is based on that described in Nimmo and Faul (2013). This model matches
88 the observed bulk density and moment of inertia of Mars; it also satisfies the measured k_2 Love
89 number and the tidal dissipation factor Q inferred from observation of Phobos' orbit. This model is
90 simplified compared with other models in which detailed mineralogical and equation of state data are
91 employed (e.g., Gudkova and Zharkov, 2004; Khan and Connolly, 2008; Rivoldini *et al.*, 2011).
92 However, compared with the enormous uncertainties in key parameters (such as the radius of the

Thorne Lay 10/3/14 7:37 PM

Deleted: allow for

Thorne Lay 10/3/14 7:38 PM

Deleted: to have

95 Martian core, and the bulk composition of the mantle), the approximations involved in our simple
96 model are unlikely to matter. Furthermore, what we are primarily concerned with here is *differences*
97 between models with and without a LVZ; such differences will not be very sensitive to changes in the
98 background model parameters.

99 Below we describe the main aspects of the velocity model in more detail. We assume that Mars
100 has differentiated into three compositionally distinct layers: the core, the mantle and the crust. We
101 also assume Mars is spherically symmetric.

102 *Crust*

103 The Martian surface is characterized by a clear topographic dichotomy, the heavily-cratered
104 southern highlands and relatively smooth northern lowlands with far fewer craters. The Martian crust
105 is non-uniform, as shown by inverting the gravity and topography data from the Mars Global
106 Surveyor (MGS) mission (Zuber, 2001). In general, the crust progressively thins from the southern
107 pole to the northern pole. For our crustal model, we use the mean value of the crustal thickness, 50
108 km, and $V_p = 6.0$ km/s, $V_s = 3.5$ km/s, density = 2900 kg/m³ (Zuber *et al.*, 2000). We set shear Q to
109 be $Q_s = 600$ and $Q_p = 9/4Q_s$.

110 *Core*

111 The Love number k_2 inferred from solar tides indicates the existence of at least an outer liquid
112 core (Yoder *et al.*, 2003). Whether Mars has a solid inner-core or not is uncertain. Existence of a solid
113 inner core will have significant effect on seismic normal mode frequencies (Okal and Anderson,
114 1978). In our model, we do not include a solid inner core. A range of core radii is permitted when
115 modeling the tidal k_2 and moment of inertia (Yoder *et al.*, 2003); we adopt a baseline value of 1650
116 km similar to that employed by Nimmo and Faul (2013). To study the mantle LVZ, the exact radius is
117 not critical. We assume 10^9 for the bulk Q in the fluid core, which means essentially no dissipation.

118 Because Nimmo and Faul (2013) were concerned primarily with dissipation in the mantle, they
119 did not calculate seismic velocities in the core. In Appendix A we outline the procedure by which the
120 core density and velocity structure were obtained.

121 *Mantle*

122 Derivation of the mantle seismic velocity and Q structure is described in detail in Nimmo and
123 Faul (2013) and only a brief summary is given here. The anelastic properties of the mantle are based
124 on experiments on Fo90 olivine conducted by Jackson and Faul (2010). To account for the fact that
125 Mars is more iron-rich than the Earth (Longhi *et al.*, 1992; Table 2 in Robinson and Taylor, 2001),
126 we treat the reference density of our mantle material as a free parameter, constrained by the moment
127 of inertia and bulk density of Mars. Iron enrichment will only increase the magnitude of any seismic
128 LVZ (Mocquet *et al.*, 1996). The temperature of the deep mantle is constrained by observations of
129 Phobos' orbital decay, which yields the bulk k_2/Q ratio (see Bills *et al.*, 2005), where Q is the tidal
130 dissipation factor at the synodic period of Phobos (~ 11.106 hours). Higher mantle temperatures and
131 smaller grain sizes result in lower values of Q . Using an extended Burgers model, the seismic
132 velocity and local Q near a seismic frequency of ~ 1.0 Hz can be derived for a specified temperature
133 profile, and a bulk tidal Q and k_2 obtained for comparison with observations. The mantle potential
134 temperature is inferred to be 1625 ± 75 K (Nimmo and Faul, 2013) for a stagnant thermal lid
135 thickness of 150 km, in good agreement with some recent petrological studies based on remote-
136 sensing observations (Baratoux *et al.*, 2011; Baratoux *et al.*, 2013). Solid phase changes, olivine-
137 wadsleyite (Earth's 410-km discontinuity) and wadsleyite-ringwoodite (Earth's 520-km
138 discontinuity) occur at Martian depths of around 1100 km and 1400 km, respectively. The precise
139 depths of these discontinuities, if obtained by seismological means in the future, could act as Martian
140 internal absolute temperature tie-points. The third phase change, ringwoodite-perovskite (or the

141 Earth's 660-km discontinuity) may or may not be present in Mars, depending on the core size and the
142 temperature in the lowermost part of the mantle.

143 Because tidal dissipation depends primarily on shear and not bulk modulus, Nimmo and Faul
144 (2013) did not present an explicit method for calculating V_p . To calculate V_p below we take the
145 mantle bulk modulus $K_m = 2G_m(1+\nu)/3(1-2\nu)$ where G_m is the (depth-dependent) shear modulus
146 obtained by Nimmo and Faul (2013) and ν is the Poisson's ratio, taken to be 0.278 which results in
147 $V_p/V_s = 1.8$ throughout the mantle. We also tested the Poisson's ratio $\nu = 0.25$ and the essential
148 diagnostics for the LVZ remain unaffected. Details of Poisson's ratio and anisotropy will only be
149 useful to address when bountiful seismic observations are obtained.

150

151 As discussed above, the main control on whether an LVZ exists is the near-surface temperature
152 gradient. A common feature of previous thermal models (Figure 1b) is that when the thermal
153 gradient is large in the lid, an LVZ exists, and vice versa. For the nominal temperature profile
154 described in Nimmo and Faul (2013), Figure 1c shows calculated elastic wave speeds and densities.
155 The Q_S model is shown in Figure 1d, with Q_P assumed to be $9/4 Q_S$.

156

157 The strong temperature increase within the stagnant thermal lid decreases seismic velocities with
158 increasing depth in the upper mantle down to a depth of about 200 km, producing a thin "seismic lid"
159 above a broad low velocity zone. To evaluate the seismological manifestations of this LVZ model,
160 we produce a similar model with the same structure at all depths below 300 km, but with no seismic
161 lid and a positive velocity increase with depth from the crust-mantle boundary, similar to earlier
162 Martian models. We label the latter model the noLVZ model, recognizing that it is likely less
163 justifiable on physical grounds than the LVZ model. Comparison of seismic wave computations for

164 the LVZ and noLVZ models isolates the effects of the thin seismic lid and the waveguide structure of
165 the associated LVZ in the lithosphere to establish the diagnostic wavefield characteristics, and makes
166 uncertainties in the deep structure relatively unimportant. Given the predicted ground motions, we
167 will then assess whether it is realistic to establish presence of an LVZ using just one 3-component
168 seismometer.

169 An important potential caveat for single-station seismology is that if the Martian interior is as
170 scattering as the lunar interior, surface waves may not be clearly recorded. However, the Moon and
171 Mars are very different bodies - particularly in terms of near-surface water content and gravity - so
172 the lunar experience does not provide much guidance in terms of what seismic waves can be
173 measured and should be expected. Direct evidence from the early Viking experiment showed that the
174 one possible recorded seismogram was more Earth-like than Moon-like (see Anderson et al., 1977).
175 Indirect evidence from geophysics indicates that the lunar interior and the Martian interior should be
176 different seismologically. Seismic scattering is caused by heterogeneities. The lunar crust is very
177 heterogeneous (and fractured) but not dissipative so that high-frequency seismic waves reverberate
178 for a very long time without much attenuation. The Martian crust is likely heterogeneous (though less
179 fractured), but is expected to be more dissipative for high-frequency seismic waves. Fractures
180 generated by impacts on Mars should be relatively compacted due to the larger gravity and presence
181 of near-surface water. The lunar mantle might be more heterogeneous than the Martian mantle
182 because of lower temperatures and lack of mantle convection (Nimmo *et al.*, 2012). Given these
183 contrasting differences between the Moon and Mars, it is useful to design and test some single-station
184 seismological methodologies before the martian seismic data are returned. On the other hand, while
185 there have been major advances in seismic instrumentation since the Apollo program, questions

Francis Nimmo 10/4/14 10:17 PM

Comment [1]: Better reference is Laneuville et al. 2013

Yingcai Zheng 9/30/14 1:55 PM

Formatted: Highlight

186 remain about how well a broadband seismometer deployed on the martian surface will resolve weak
187 long-period motions.

188 **3. Seismological signature of a lithospheric LVZ**

189 Seismological studies of the Martian interior will require seismic sources producing sufficient
190 elastic wave energy and high quality broadband seismometers. It is not clear what types or numbers
191 of seismic sources exist on Mars. As reviewed by Lognonne and Johnson (2007), possible sources
192 include potential marsquakes due to brittle faulting (Golombek *et al.*, 1992; Knapmeyer *et al.*, 2006;
193 Taylor *et al.*, 2013), asteroid impacts (Teanby and Wookey, 2011; Daubar *et al.*, 2013), tidal loading,
194 landslides, atmospheric hum, Chandler wobble, etc. (Solomon *et al.*, 1991). During the 19 months of
195 operation of the short-period seismometer on the Viking 2 lander, only atmospheric noise and maybe
196 one marsquake were recorded (Anderson *et al.*, 1977). Better ground coupling, sensitivity, and broad
197 frequency range may allow us to observe signals from other types of sources. In this paper, we
198 assume that an energetic source will occur and can be recorded by the broadband seismometer with
199 good signal-to-noise for periods from 1 to 150 s.

200 For the LVZ and noLVZ models, we computed seismic wave attributes by a suite of methods,
201 including conventional ray theory (Cerveny, 2005), normal mode theory (Aki and Richards, 1980;
202 Woodhouse, 1988) and frequency-wavenumber (or angular order, in spherical coordinates)
203 integration methods (Fuchs and Muller, 1971; Geller and Ohminato, 1994). We will not go into
204 details about the methods as they are well established, and we confirmed compatibility of calculations
205 for the various methods for specific sources and epicentral distances. To calculate the mode
206 frequencies, we used the MINEOS code (Masters *et al.*, 2011) and benchmarked its full waveforms
207 with the Direct Solution Method (DSM) (Geller and Ohminato, 1994; Takeuchi *et al.*, 1996). The

208 normal mode method first searches for eigenfrequencies and their associated eigenfunctions and then
209 expands the source force function onto those eigenfunctions to find the source excitation terms.
210 Searching for the eigenfrequencies can be time consuming at high frequency as adjacent
211 eigenfrequencies can be very close to each other. Normal modes are used to synthesize low-frequency
212 (shortest period of ~ 16 s) seismograms. The DSM does not depend on root searching and can
213 compute high frequency waves. Here we focus on the resulting wavefield characteristics.

214 *Body waves*

215 For a shallow seismic source in the crust (here we use 0 km depth), the most distinct signature of
216 the LVZ model relative to noLVZ is the shadow zone for direct P (or S) wave (Figure 2a,c) spanning
217 the epicentral distance range of 20° to 55° (Figure 2b,d). Gutenberg discovered Earth's LVZ by
218 modeling the direct-wave amplitudes at different epicentral distances for which seismic rays traverse
219 the LVZ (Gutenberg, 1959), but he had the advantage of having sources at intermediate depths within
220 subducting slabs, which will not be present in the stagnant Martian lid. The shadow zone appears
221 obvious, but in practice, diffraction along the crust-mantle boundary and misidentification of
222 secondary phases such as PP complicate the interpretation. Multiple sources at a wide range of
223 epicentral distances could allow some confidence in the detection of the shadow zone, but full-
224 waveform computation for the LVZ and noLVZ models indicates that the presence of a LVZ causes
225 little identifiable difference in *long-period body waves* (Figure 3). While frequency dependence of
226 the waveforms might resolve the nature of the diffracted energy that fills the seismic shadow, it is
227 likely this will not be viable if only a few sources are available.

228 *Normal Modes*

229 Normal modes probe Mars as an entire planet (e.g., Gudkova and Zharkov, 2004), which is
230 attractive given a small number of sensors, but challenging for resolving a localized upper mantle

Yingcai Zheng 9/29/14 10:49 AM

Deleted: The ray tracing calculations in Figure 2 indicate an interesting feature of PKP waves that traverse the liquid core. If the Martian core is about 1650 km in radius as in our model, the antipodal seismic PKP-wave focusing is likely to be very strong since the PKP-b caustic locates very close to the antipode. This is true whether there is an LVZ (or a solid inner core) or not. Antipodal seismic focusing may induce chaotic terrains such as in the case of Caloris impact on Mercury (Schultz and Gault, 1975; Lu *et al.*, 2011) and some basins on Mars (Williams and Greeley, 1994). To further constrain the core size, multiple ScS reverberations might be used (Revenaugh and Jordan, 1991).

247 structural feature. Normal-mode seismology analyzes the vibrational eigenfrequencies of a planet (or
248 the Sun in helioseismology) for a long recording of ground motion, assuming there is a sufficient
249 single or continuous source of excitation. A single station may suffice for this purpose. If the gravest
250 normal modes (e.g., angular order < 10) of Mars can be excited and identified, they can reveal
251 whether the core is liquid or solid (Okal and Anderson, 1978). The period of, ${}_0S_2$, the longest period
252 mode, is 2260 seconds for the LVZ model. For the noLVZ model, the period of ${}_0S_2$ is 2267 seconds.
253 If the core is solid, this period can be much shorter (around 1000 s, depending on the structure), thus
254 for the purpose of detecting the LVZ, the low frequency mode frequencies will not be diagnostic. For
255 low angular orders less than 10, the frequency shifts due to an LVZ are very small for spheroidal,
256 toroidal and radial modes (Figure 4). However, frequency shifts are significant for large ℓ for
257 fundamental modes and overtones. Identification of the modes for a single seismometer will be
258 challenging and constrained by the source distribution and characteristics. However, it is possible to
259 measure surface wave dispersion for those modes using a single seismometer.

260 *Surface waves*

261 Dispersion of intermediate period (30-150 s) mantle Rayleigh or Love waves is likely to be the
262 most diagnostic observable for the existence of the LVZ (Figure 5). For Rayleigh waves, there is a
263 pronounced Airy phase (minima or maxima in the group velocity curve) around a period of 100 s, for
264 the LVZ model, along with significant overall shifts to higher phase and group velocities due to the
265 presence of the seismic lid. For the noLVZ model, the Rayleigh wave group velocity increases
266 monotonically beyond the crustal Airy phase located around 30s. For different lid thicknesses (80km
267 and 160km), Rayleigh wave dispersion curves are different (Figure 6), with thicker lids giving faster
268 group velocities and shifting the Airy phase to longer periods. The differences in dispersion give
269 cumulative waveform differences that are substantial. Figure 7 compares Rayleigh and Love

270 waveforms at distances of 30° and 60° from a double-couple shear dislocation at a depth of 10 km for
271 the LVZ and noLVZ models [and large time-domain differences in Rayleigh waves are due to the](#)
272 [mantle Airy phase. The maximum in the group-velocity dispersion was also recognized by Panning et](#)
273 [al. \(2006\) as a way of probing Europa's ice shell structure.](#) Assuming that an event's approximate
274 location can be deduced from relative times of body wave arrivals and signal polarization information
275 (with identification of the great-circle path based on separation of Love and Rayleigh motions or
276 body wave polarizations), it should be possible to evaluate the dispersion in either time or frequency
277 domain to test the likelihood of LVZ existence. Given a single seismometer and a large energy
278 source somewhere on the planet, global-circling surface Rayleigh waves, R1, R2, R3, ..., Rn
279 (likewise, G1, G2, G3, ..., Gn for Love waves) can be used to deduce the global average dispersion
280 curves with high fidelity (Satô, 1958; p.381 in Aki and Richards, 1980; [Panning et al., 2012](#))
281 provided the polar phase shift is taken into account (Brune et al., 1961) (see Figures S1-S3 for single-
282 station based dispersion measurement at different epicentral distances). With the specification of the
283 InSight seismometer, it is estimated that about 20 events may have enough energy to excite global
284 surface waves over the operational period of 720 days (Lognonne et al., 2012). Taylor et al. (2013)
285 estimated a high likelihood of having tens of M_w 5.0 events in the Cerberus Fossae region per Earth's
286 year. [For the seismic event in Figure 3, our calculations show that R1-R5 Rayleigh waves are above](#)
287 [the instrument sensitivity and projected Martian wind noise \(Lognonne et al., 2012\).](#) If this is the case,
288 we would be able to determine the existence of the LVZ using a single seismometer [if high signal-to-](#)
289 [noise broadband recordings are recovered. There is no question that complexities such as radial](#)
290 [anisotropy and 3D crustal and lithospheric structure can complicate the waveforms and possibly](#)
291 [overwhelm the diagnostic differences we propose for simple 1D models. Even for the Earth, there is](#)

Francis Nimmo 10/4/14 10:28 PM

Deleted: used

Thorne Lay 10/3/14 7:39 PM

Deleted: to study

Francis Nimmo 10/4/14 10:28 PM

Deleted: to predict

Yingcai Zheng 9/29/14 10:57 AM

Deleted: In the time domain, the global seismic wavefields for the LVZ and noLVZ models for a double couple source at 10 km depth (Figure 8) show how distinct the ground motions will be at all distances, presumably enabling robust detection of an LVZ even from sparse source distributions.

Thorne Lay 10/3/14 7:40 PM

Deleted: s

303 | [difficulty in resolving LVZ attributes with sparse data sets, so we do not want to be overly optimistic,](#)
304 | [but everything hinges on the uncertain nature of the data and sources that will be observed.](#)

305 **4. Conclusions**

306 The possible existence of a pronounced seismic low velocity zone (LVZ) in the uppermost mantle
307 of Mars is indicated because of the increased importance of thermal relative to pressure effects on
308 velocity in the lithosphere of this low-gravity planet. Thermal models consistent with convection
309 simulations and the inferred tidal Q of Mars predict a thin seismic lid below the crust-mantle
310 boundary, with a pronounced LVZ extending several hundred kilometers across the thermal
311 lithosphere. Based on seismological modeling for the resulting Mars seismic velocity structure, we
312 find that the strongest indication of the presence of a lithospheric LVZ will be provided by dispersion
313 characteristics of Rayleigh waves. This is due to the development of long-period Airy phases for
314 structures with an LVZ. Single station observations of long-period dispersion for events that are
315 approximately located should be viable as long as the sources are large enough to give good signal-
316 to-noise ratio long-period surface wave observations. The broadband three-component seismometer
317 to be deployed by NASA's InSight mission in 2016 may provide an opportunity to verify the
318 existence of an LVZ in the Martian upper mantle. Doing so will provide valuable information for
319 constraining Martian internal thermal evolution, volatile content and dynamics.

320 **5. Acknowledgments**

321 | YZ thanks ERL/MIT for [facilities](#) support to carry out this work. T. Lay is supported by NSF grant
322 | EAR-1245717.

323

324 **Appendix A.**

325 Below we outline a prescription for calculating the sound-speed inside the core (assumed liquid). This
326 approach is significantly simplified compared with some other work (e.g., Gudkova and Zharkov,
327 2004; Khan and Connolly, 2008; Rivoldini *et al.*, 2011). Our rationale for a simplified approach is
328 twofold. First, the errors introduced by our approach are very small compared to major uncertainties
329 in the bulk structure of Mars (such as the core radius). Second, we are focusing here primarily on the
330 role of the mantle LVZ, so that our core velocity structure is of only secondary interest.

331 The pressure at the base of the mantle P_{cmb} is given by (e.g., Nimmo and Faul, 2013)

$$332 \quad P_{cmb} = \frac{4}{3}\pi G \rho_m \left[R_c^3 \Delta\rho \left(\frac{1}{R_c} - \frac{1}{R} \right) + \frac{\rho_m}{2} (R^2 - R_c^2) \right]$$

333 Here R_c is the core radius, ρ_m is the mantle density, $\Delta\rho$ is the core-mantle density contrast, R is the
334 planetary radius, and G is the gravitational constant. This expression is approximate because it
335 assumes a constant mantle density (constrained by the bulk density and moment of inertia of Mars).
336 The errors introduced by this approximation are a few percent, very small compared to other
337 uncertainties regarding the bulk structure of Mars (see Nimmo and Faul, 2013). The pressure at a
338 radial position r within the core is then given by

$$339 \quad P(r) = P_{cmb} + \frac{2}{3}\pi G \rho_c^2 (R_c^2 - r^2)$$

340
341 A constant core density ρ_c is assumed here (constrained by the bulk density and moment of inertia).
342 Again, the error introduced by this approximation is small compared to other uncertainties, especially
343 because the pressure (and thus density) change across the Martian core is modest. In calculating the
344 velocity profile within the core, we do allow the density to vary (see below). The temperature profile
345 within the core $T(r)$ is assumed to be adiabatic:

346 $T(r) = T_{cmb} \exp\left(\frac{[R_c^2 - r^2]}{D^2}\right)$

347 where T_{cmb} is the temperature at the core-mantle boundary and D is a length scale given by (e.g.,
 348 Labrosse *et al.*, 2001)

349 $D = \left(\frac{3C_p}{2\pi\alpha G\rho_c}\right)^{1/2}$

350 where α is the thermal expansivity and C_p is the specific heat capacity (both assumed constant). We
 351 take the bulk modulus at the core-mantle boundary (CMB) to be K_c . The bulk modulus inside the core
 352 is then calculated using a linear approximation (because the changes in T and P are small):

353 $K_c(r) = K_c + (P(r) - P_{cmb})\frac{dK_c}{dP} + (T(r) - T_{cmb})\frac{dK_c}{dT}$

354 Similarly, taking the density at the CMB to be ρ_c , the variation of density inside the core is calculated
 355 using

356 $\rho(r) = \rho_c \left(1 + \frac{P(r) - P_{cmb}}{K_c}\right) (1 - \alpha[T(r) - T_{cmb}])$

357 The P-wave velocity is then simply given by $V_p(r) = [K_c(r)/\rho(r)]^{1/2}$.

358
 359 The core properties were obtained from the FeS end-member of Bertka and Fei (1998) and the
 360 compilation of Williams and Nimmo (2004). The value of K_c was derived from the one-bar value of
 361 54 GPa and dK_c/dP . The value of T_{cmb} assumed is not critical, because the temperature contrast across
 362 the core matters much more than the absolute temperature. Mantle and bulk properties are from the
 363 reference model described in Nimmo and Faul (2013).

364

Quantity	Value	Units	Reference	Quantity	Value	Units	Reference
R_c	1650	km	-	ρ_c	7000	kg m ⁻³	1
K_c	134	GPa	See text	dK_c/dP	4	-	2
dK_c/dT	-0.02	GPa K ⁻¹	2	C_p	780	J kg ⁻¹ K ⁻¹	3
T_{cmb}	2500	K	3	α	5.85×10^{-5}	K ⁻¹	3
ρ_m	3526	kg m ⁻³	1				

365 Table A1. Quantities used in construction of core velocity model. References are: (1) Nimmo and

366 Faul (2013); (2) Bertka and Fei (1998); (3) Williams and Nimmo (2004).

367

References

- 369
370
371 Aki, K., and P. G. Richards (1980), *Quantitative Seismology*, Freeman and Co., San Francisco.
372 Anderson, D. L. (1989), *Theory of the Earth*, Blackwell Scientific Publications, Boston.
373 Anderson, D. L., W. F. Miller, G. V. Latham, Y. Nakamura, M. N. Toksöz, A. M. Dainty, F. K.
374 Duennebieer, A. R. Lazarewicz, R. L. Kovach, and T. C. D. Knight (1977), Seismology on
375 Mars, *J. Geophys. Res.*, **82**(28), 4524-4546.
376 Banerdt, W. B., S. Smrekar, K. Hurst, P. Lognonne, T. Spohn, S. Asmar, D. Banfield, L. Boschi, U.
377 Christensen, V. Dehant, W. Folkner, D. Giardini, W. Goetz, M. Golombek, M. Grott, T.
378 Hudson, C. Johnson, G. Kargl, N. Kobayashi, J. Maki, D. Mimoun, A. Mocquet, P. Morgan,
379 M. Panning, W. T. Pike, J. Tromp, T. van Zoest, R. Weber, and M. Wieczorek (2013),
380 InSight: a Discovery mission to explore the interior of Mars, *Lunar and Planetary Science*
381 *Conference*, **44**, 1915.
382 Baratoux, D., M. J. Toplis, M. Monnereau, and O. Gasnault (2011), Thermal history of Mars inferred
383 from orbital geochemistry of volcanic provinces (vol 472, pg 338, 2011), *Nature*, **475**(7355),
384 254-254.
385 Baratoux, D., M. J. Toplis, M. Monnereau, and V. Sautter (2013), The petrological expression of
386 early Mars volcanism, *Journal of Geophysical Research-Planets*, **118**(1),
387 10.1029/2012JE004234.
388 Bertka, C. M., and Y. Fei (1997), Mineralogy of the Martian interior up to core-mantle boundary
389 pressures, *Journal of Geophysical Research: Solid Earth*, **102**(B3), 5251-5264.
390 Bertka, C. M., and Y. W. Fei (1998), Density profile of an SNC model Martian interior and the
391 moment-of-inertia factor of Mars, *Earth Planet. Sci. Lett.*, **157**(1-2), 79-88.
392 Bills, B. G., G. A. Neumann, D. E. Smith, and M. T. Zuber (2005), Improved estimate of tidal
393 dissipation within Mars from MOLA observations of the shadow of Phobos, *Journal of*
394 *Geophysical Research-Planets*, **110**(E7).
395 Brune, J. N., J. E. Nafe, and L. E. Alsop (1961), The polar phase shift of surface waves on a sphere,
396 *Bull. Seismol. Soc. Am.*, **51**(2), 247-257.
397 Cervený, V. (2005), *Seismic Ray Theory*, 724 pp., Cambridge University Press, Cambridge, UK.
398 Daubar, I. J., A. S. McEwen, S. Byrne, M. R. Kennedy, and B. Ivanov (2013), The current martian
399 cratering rate, *Icarus*, **225**(1), 506-516.
400 Franck, S., and G. Kowalle (1994), Seismic velocity models for an internally asymmetric Mars, *Earth*
401 *Moon and Planets*, **65**(3), 277-290.
402 Fuchs, K., and G. Muller (1971), Computation of synthetic seismograms with the reflectivity method
403 and comparison with observations, *Geophys J Int*, **23**(4), 417-433.
404 Geller, R. J., and T. Ohminato (1994), Computation of synthetic seismograms and their partial
405 derivatives for heterogeneous media with arbitrary natural boundary-conditions using the
406 direct solution method, *Geophys. J. Int.*, **116**(2), 421-446.
407 Golombek, M. P., W. B. Banerdt, K. L. Tanaka, and D. M. Tralli (1992), A prediction of Mars
408 seismicity from surface faulting, *Science*, **258**(5084), 979-981.
409 Gudkova, T. V., and V. N. Zharkov (2004), Mars: interior structure and excitation of free oscillations,
410 *Phys. Earth Planet. Inter.*, **142**(1-2), 1-22.
411 Gutenberg, B. (1948), On the layer of relatively low wave velocity at a depth of about 80 kilometers,
412 *Bull. Seismol. Soc. Am.*, **38**(2), 121-148.

413 Gutenberg, B. (1959), *Physics of the Earth's Interior*, Springer, New York.

414 Jackson, I., and U. H. Faul (2010), Grainsize-sensitive viscoelastic relaxation in olivine: Towards a
415 robust laboratory-based model for seismological application, *Phys. Earth Planet. Inter.*,
416 **183**(1–2), 151-163.

417 Khan, A., and J. A. D. Connolly (2008), Constraining the composition and thermal state of Mars from
418 inversion of geophysical data, *Journal of Geophysical Research-Planets*, **113**(E7).

419 Knapmeyer, M., J. Oberst, E. Hauber, M. Wahlich, C. Deuchler, and R. Wagner (2006), Working
420 models for spatial distribution and level of Mars' seismicity, *Journal of Geophysical
421 Research-Planets*, **111**(E11).

422 Labrosse, S., J. P. Poirier, and J. L. Le Mouel (2001), The age of the inner core, *Earth Planet. Sci.
423 Lett.*, **190**(3-4), 111-123.

424 Lognonne, P., W. B. Banerdt, K. Hurst, D. Mimoun, R. Garcia, M. Lefevre, J. Gagnepain-Beyneix,
425 M. Wiezorek, A. Mocquet, M. Panning, E. Beucler, S. Deraucourt, D. Giardini, L. Boschi, U.
426 Christensen, W. Goetz, T. Pike, C. Johnson, R. Weber, K. Larmat, N. Kobayashi, and J.
427 Tromp (2012), InSight and single-station broadband seismology; from signal and noise to
428 interior structure determination, *Lunar and Planetary Science Conference*, **43**, 1983.

429 Lognonne, P., and C. Johnson (2007), Planetary Seismology, in *Treatise on Geophysics*, edited, pp.
430 69-122, Elsevier, Amsterdam.

431 Longhi, J., E. Knittle, J. R. Holloway, and H. Wanke (1992), The bulk composition, mineralogy and
432 internal structure of Mars, in *in Mars*, edited by H. H. Kieffer, et al., pp. 184–208 Univ.
433 Arizona Press, Tucson.

434 Lu, J. N., Y. S. Sun, M. N. Toksoz, Y. C. Zheng, and M. T. Zuber (2011), Seismic effects of the
435 Caloris basin impact, Mercury, *Planet Space Sci*, **59**(15), 1981-1991.

436 Masters, G., M. Barmine, and S. Kientz (2011), Mineos (version 1.0.2), *Computational Infrastructure
437 for Geodynamics (CIG)*, <http://www.geodynamics.org> last accessed 2/10/2014. .

438 Mocquet, A., and M. Menvielle (2000), Complementarity of seismological and electromagnetic
439 sounding methods for constraining the structure of the Martian mantle, *Planet Space Sci*,
440 **48**(12-14), 1249-1260.

441 Mocquet, A., P. Vacher, O. Grasset, and C. Sotin (1996), Theoretical seismic models of Mars: The
442 importance of the iron content of the mantle, *Planet Space Sci*, **44**(11), 1251-1268.

443 Nimmo, F., and U. H. Faul (2013), Dissipation at tidal and seismic frequencies in a melt-free,
444 anhydrous Mars, *J. Geophys. Res. Planets*, **118**, 2558-2569.

445 Nimmo, F., U. H. Faul, and E. J. Garnero (2012), Dissipation at tidal and seismic frequencies in a
446 melt-free Moon, *Journal of Geophysical Research-Planets*, **117**.

447 Ogawa, M., and T. Yanagisawa (2011), Numerical models of Martian mantle evolution induced by
448 magmatism and solid-state convection beneath stagnant lithosphere, *Journal of Geophysical
449 Research: Planets*, **116**(E8), E08008.

450 Okal, E. A., and D. L. Anderson (1978), Theoretical models for Mars and their seismic properties,
451 *Icarus*, **33**, 514-528.

452 Panning, M., V. Lekic, M. Manga, F. Cammarano, and B. Romanowicz (2006), Long-period
453 seismology on Europa: 2. Predicted seismic response, *Journal of Geophysical Research:
454 Planets*, **111**(E12), E12008.

455 Panning, M. P., A. Mocquet, E. Beucler, W. B. Banerdt, P. Lognonne, L. Boschi, C. Johnson, R. C.
456 Weber, and Anonymous (2012), InSight; using Earth data to demonstrate inversion techniques
457 for Mars' interior, *Abstracts of Papers Submitted to the Lunar and Planetary Science
458 Conference*, **43**, 0-Abstract 1515.

459 Revenaugh, J., and T. H. Jordan (1991), Mantle layering from ScS reverberations .1. Waveform
460 inversion of zeroth-order reverberations, *Journal of Geophysical Research-Solid Earth*,
461 **96**(B12), 19749-19762.

462 Rivoldini, A., T. Van Hoolst, O. Verhoeven, A. Mocquet, and V. Dehant (2011), Geodesy constraints
463 on the interior structure and composition of Mars, *Icarus*, **213**(2), 451-472.

464 Robinson, M. S., and G. J. Taylor (2001), Ferrous oxide in Mercury's crust and mantle, *Meteoritics &*
465 *Planetary Science*, **36**(6), 841-847.

466 Satô, Y. (1958), Attenuation, dispersion, and the wave guide of the G wave, *Bull. Seismol. Soc. Am.*,
467 **48**(3), 231-251.

468 Schultz, P. H., and D. E. Gault (1975), Seismic effects from major basin formations on the moon and
469 Mercury, *The Moon*, **12**, 159-177.

470 Sohl, F., and T. Spohn (1997), The interior structure of Mars: Implications from SNC meteorites,
471 *Journal of Geophysical Research-Planets*, **102**(E1), 1613-1635.

472 Solomon, S. C., D. L. Anderson, W. B. Banerdt, R. G. Butler, P. M. Davis, F. K. Duennebier, Y.
473 Nakamura, E. A. Okal, and R. J. Phillips (1991), Scientific Rationale and Requirements for a
474 Global Seismic Networks on Mars, LPI Tech. Rpt, 91-02,51 pp, Lunar and Planetary Institute,
475 Houston.

476 Stixrude, L., and C. Lithgow-Bertelloni (2005), Mineralogy and elasticity of the oceanic upper
477 mantle: Origin of the low-velocity zone, *Journal of Geophysical Research-Solid Earth*,
478 **110**(B3), -.

479 Takeuchi, N., R. J. Geller, and P. R. Cummins (1996), Highly accurate P-SV complete synthetic
480 seismograms using modified DSM operators, *Geophys. Res. Lett.*, **23**(10), 1175-1178.

481 Taylor, J., N. A. Teanby, and J. Wookey (2013), Estimates of seismic activity in the Cerberus Fossae
482 region of Mars, *Journal of Geophysical Research: Planets*, n/a-n/a.

483 Teanby, N. A., and J. Wookey (2011), Seismic detection of meteorite impacts on Mars, *Phys. Earth*
484 *Planet. Inter.*, **186**(1-2), 70-80.

485 Toksöz, M. N., and A. T. Hsui (1978), Thermal history and evolution of Mars, *Icarus*, **34**(3), 537-
486 547.

487 Verhoeven, O., A. Rivoldini, P. Vacher, A. Mocquet, G. Choblet, M. Menvielle, V. Dehant, T. Van
488 Hoolst, J. Sleewaegen, J. P. Barriot, and P. Lognonne (2005), Interior structure of terrestrial
489 planets: Modeling Mars' mantle and its electromagnetic, geodetic, and seismic properties,
490 *Journal of Geophysical Research-Planets*, **110**(E4).

491 Walzer, U., T. Burghardt, R. Hendel, and J. Kley (2010), *Towards a Dynamical Model of Mars'*
492 *Evolution*, 485-510 pp.

493 Williams, D. A., and R. Greeley (1994), Assessment of Antipodal-Impact Terrains on Mars, *Icarus*,
494 **110**(2), 196-202.

495 Williams, J. P., and F. Nimmo (2004), Thermal evolution of the Martian core: Implications for an
496 early dynamo, *Geology*, **32**(2), 97-100.

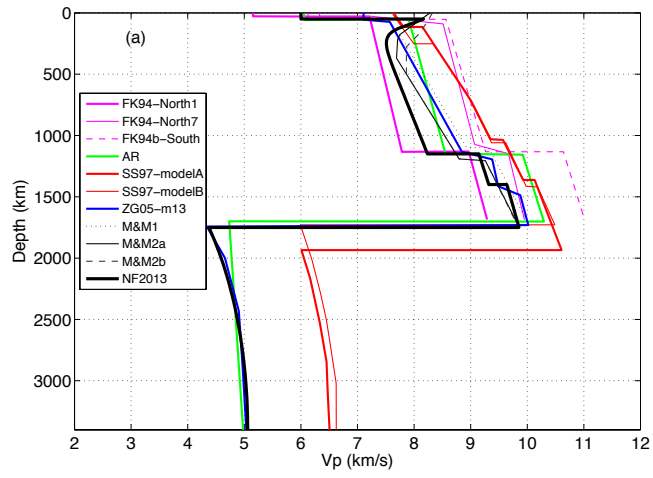
497 Woodhouse, J. (1988), The calculations of eigenfrequencies and eigenfunctions of the free
498 oscillations of the Earth and the Sun, in *Seismological Algorithms, Computational Methods*
499 *and Computer Programs*, edited by D. J. Doornbos, pp. 321-370, Academic Press, London,
500 UK.

501 Yoder, C. F., A. S. Konopliv, D. N. Yuan, E. M. Standish, and W. M. Folkner (2003), Fluid Core
502 Size of Mars from Detection of the Solar Tide, *Science*, **300**(5617), 299-303.

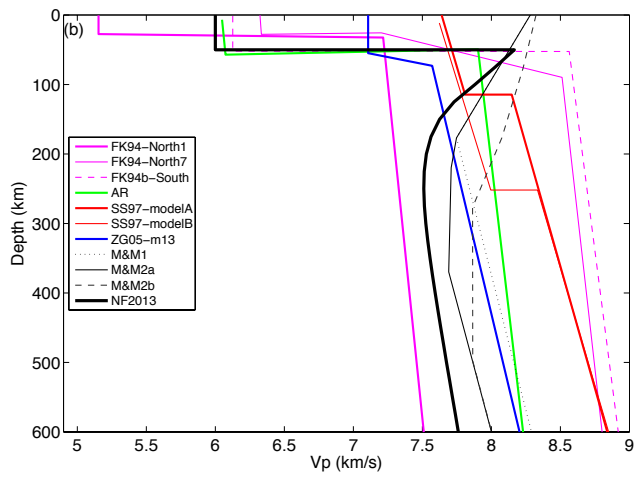
503 Zharkov, V. N., and T. V. Gudkova (2005), Construction of Martian interior model, *Sol Syst Res*,
504 **39**(5), 343-373.

505 Zuber, M. T. (2001), The crust and mantle of Mars, *Nature*, **412**(6843), 220-227.
506 Zuber, M. T., S. C. Solomon, R. J. Phillips, D. E. Smith, G. L. Tyler, O. Aharonson, G. Balmino, W.
507 B. Banerdt, J. W. Head, C. L. Johnson, F. G. Lemoine, P. J. McGovern, G. A. Neumann, D.
508 D. Rowlands, and S. J. Zhong (2000), Internal structure and early thermal evolution of Mars
509 from Mars Global Surveyor topography and gravity, *Science*, **287**(5459), 1788-1793.
510

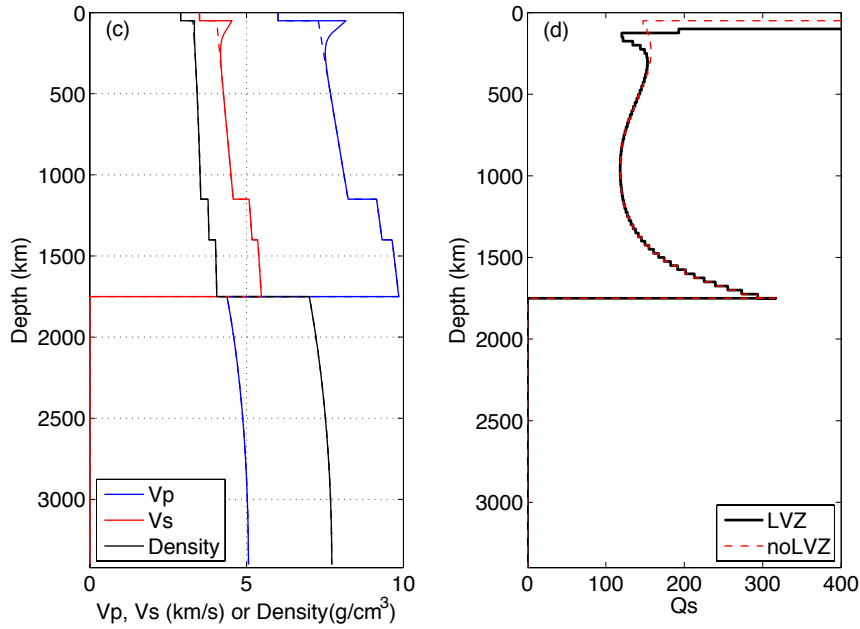
511



512

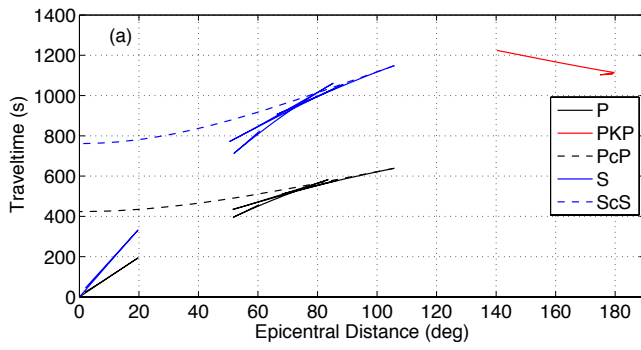


513

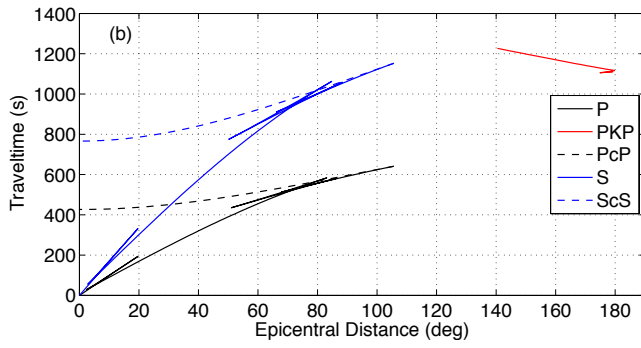


514
515

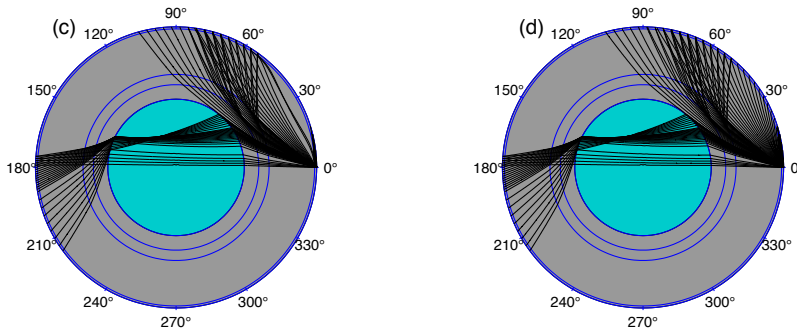
516 Figure 1. (a) Representative Martian seismicological models (V_p) showing no LVZs: FK94-North1,-
 517 North7,-South (Franck and Kowalle, 1994), AR (Okal and Anderson, 1978), SS97-modelA&B (Sohl
 518 and Spohn, 1997); and models with LVZs: M&M1,2a,2b (Mocquet and Menvielle, 2000), and model
 519 NF2013 (Nimmo and Faul, 2013). (b) Zoomed-in for the upper 600km of modes in (a); (c) Seismic
 520 velocities: V_p (blue), V_s (red), and density (black) for LVZ model (solid lines) and for noLVZ
 521 model (dash lines). Olivine phase transitions are included and give mantle discontinuities. (d)
 522 Q_s at 1.0 Hz for the LVZ model and noLVZ model. Tabulated model parameters for LVZ and noLVZ
 523 are in Table S1 and S2 in the supplementary online materials.



524



525



526

527

528

529

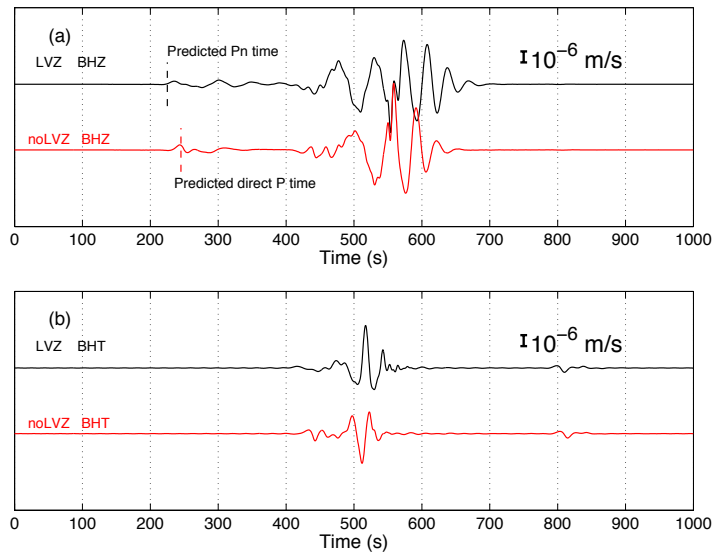
530

531

532

Figure 2. Traveltime curves for LVZ (a) and noLVZ (b). Notice the direct P shadow in the range of 20-44 degrees caused by the LVZ (a); and seismic rays for direct P (in the mantle) and PKP (through the core) phases for the LVZ (c) and noLVZ (d) models.

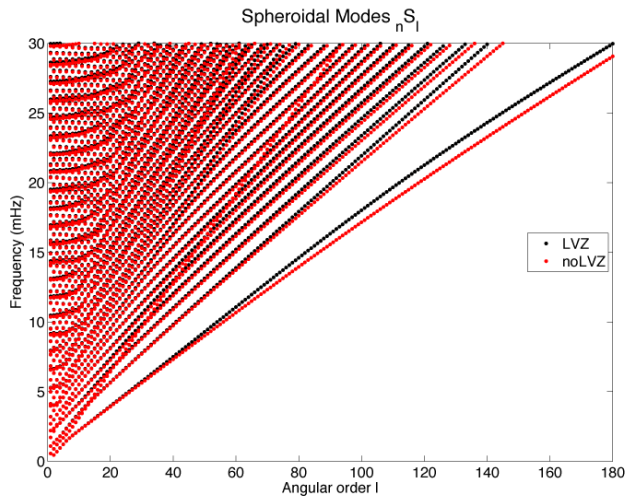
533
534



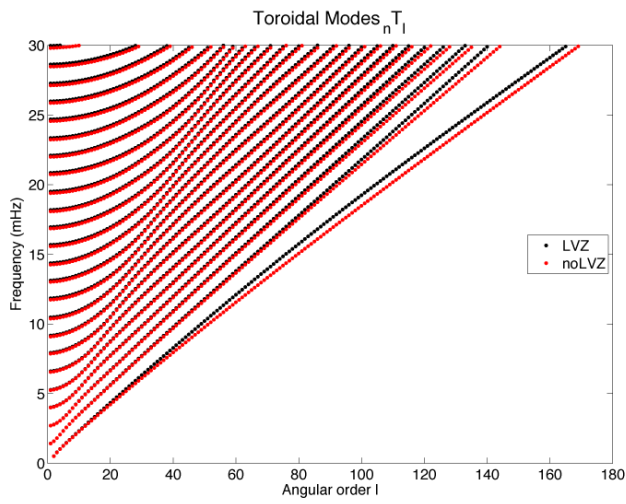
535

536
537
538
539
540
541
542
543
544
545

Figure 3. Vertical (BHZ) and tangential (BHT) components of velocity seismograms at epicentral distance of 30° , bandpass-filtered between 200 s and 25 s, for LVZ and noLVZ models. The seismic moment is 10^{18} Nm. The marsquake is a thrust event on a fault plane with strike 45° , dip 45° and rake 90° . The seismic moment is 10^{18} Nm. The epicenter is at (0° E, 0° N) and the source depth is 10km. The receiver is located at (30° E, 0° N).



546

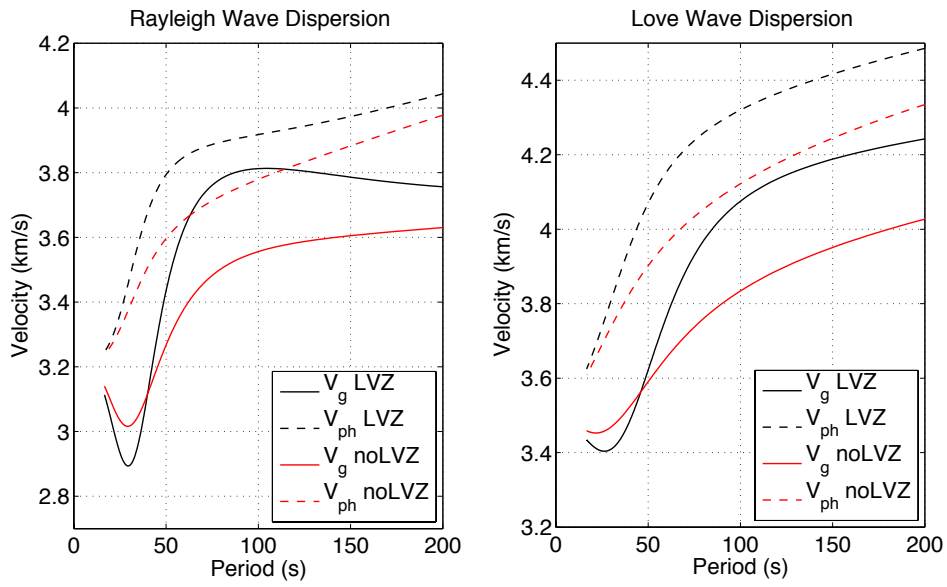


547

548

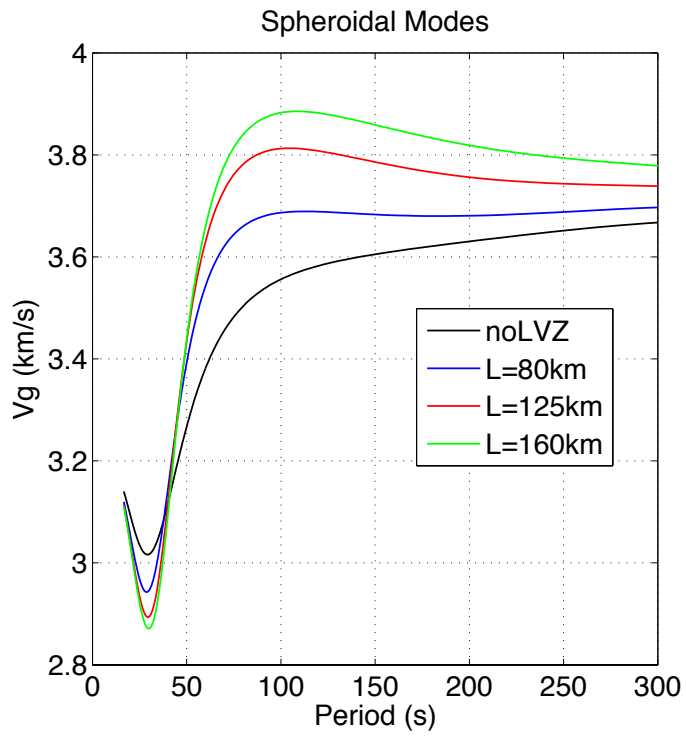
549

Figure 4. Spheroidal and toroidal mode eigenfrequencies for LVZ and noLVZ models.

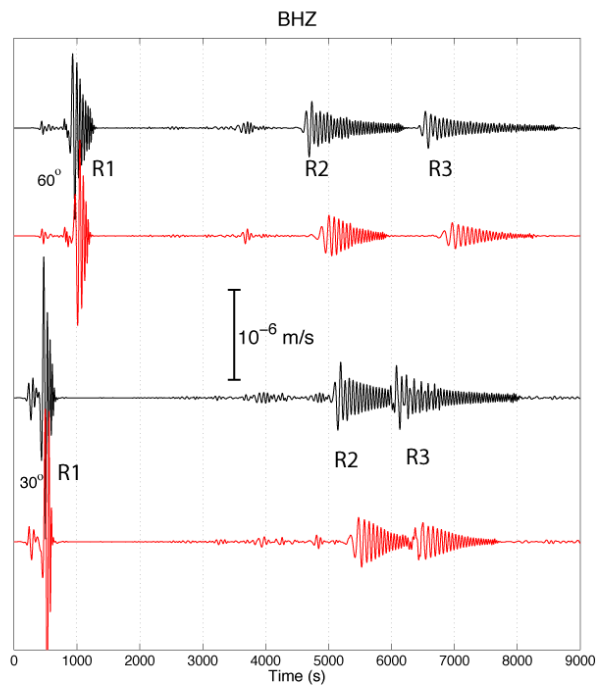


550
551
552
553

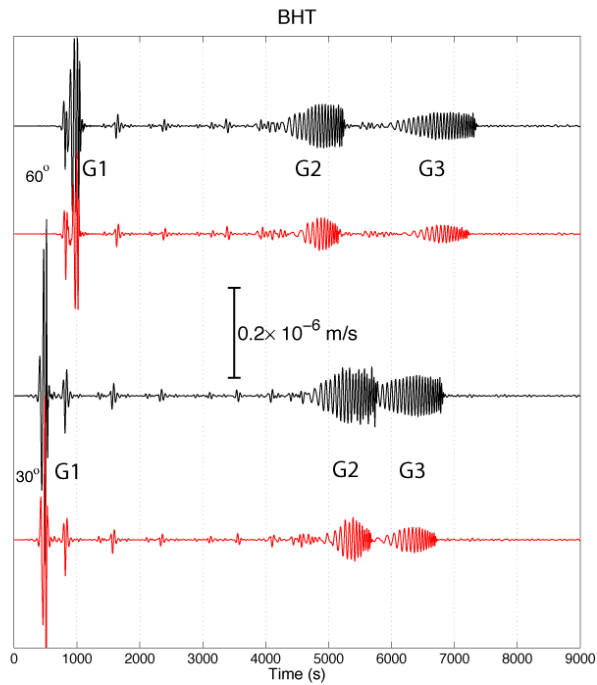
Figure 5. Dispersion curves of phase (V_{ph}) and group (V_g) velocities for fundamental Rayleigh and Love modes for the LVZ and noLVZ models.



554
 555 Figure 6. Fundamental-mode Rayleigh-wave group velocities for Martian seismic velocity models
 556 with different lid thicknesses, L .
 557
 558



559



560
 561 Figure 7. Globally traversing Rayleigh (BHZ component; top) and Love (BHT component; bottom)
 562 waves for LVZ (black) and noLVZ (red) models at three different distances. The waveforms are
 563 bandpass filtered between 200 s and 50 s using a Butterworth filter with two passes and two poles.
 564 The marsquake is a thrust event on a fault plane with strike 45°, dip 45° and rake 90°. The seismic
 565 moment is 10^{18} Nm. The epicenter is at (0°E, 0°N) and the source depth is 10km. The receivers are
 566 located at (30°E, 0°N) and (60°E, 0°N).
 567

Yingcai Zheng 9/29/14 10:57 AM
 Deleted: [1]